Supplementary Information: Density profile of ^{3}He in a nanoscale ^{3}He -^{4}He superfluid film determined by neutron scattering

Oleg Kirichek,* Christopher R. Lawson, Christy J. Kinane, Andrew J. Caruana, and Sean Langridge
ISIS Neutron and Muon Source, Rutherford Appleton Laboratory, Harwell Science and Innovation Campus, Oxon, OX11 0QX, United Kingdom.

Timothy R. Charlton
Neutron Sciences Division, Oak Ridge National Laboratory, Oak Ridge, Tennessee 37831, United States

Peter V. E. McClintock
Department of Physics, Lancaster University, Lancaster, LA1 4YB, United Kingdom
(Dated: May 24, 2024)

Supplementary Note 1: Helium Densities as a Function of Temperature

To calculate the initial estimates for the scattering length densities of the ^{4}He and ^{3}He-^{4}He mixture, it was necessary to have good estimates of their densities as functions of temperature. These data, reproduced from the work in references [1, 2], are shown in Supplementary Figure 1. The values for the lowest temperatures measured in the pure ^{4}He and ^{3}He-^{4}He mixture, were used to seed the initial neutron fits.

Supplementary Note 2: Specular Data Analysis

The primary analysis of the neutron reflectivity (NR) data was performed using the *Refl1D* software package from the National Center for Neutron Research (NCNR) at the National Institute for Standards and Technology (NIST) [3]. *Refl1D* uses the Bayesian analysis fitting package Bumps [4], both for obtaining the best fit and for performing an uncertainty analysis on the parameters used to model the data. *Refl1D* is based on the Abeles optical matrix method [5] along with interfaces approximated using the method of Névot and Croce [6].

Refl1D allows multiple data sets to be fitted simultaneously which is advantageous in this case. Liquid Helium of either isotope has very little neutron contrast as compared to air, with both having an SLD a factor two smaller than that of Si and SiO_2 as shown in Supplementary Table I.

Analysis of specular reflectivity data has several challenges. Principally, when fitting a single data set there can exist multiple profiles that give the same result due to the loss of phase information [7].

Here we cannot vary the neutron contrast but we can characterize the Si block without any Helium in the system, such that it just has a vacuum above the surface.

Isotope	b (fm)	Density (g/cm^3)	SLD (x10^{-6} Å^{-2})
Air	0	0	0
Si	4.1491	2.330	2.074
SiO_2	15.7551	2.196	3.469
^{3}He	5.74-1.483i	0.08172	0.9366
^{4}He	3.26	0.14511	0.7117
Solid ^{4}He	3.26	0.187	0.9172

Supplementary Table I: The scattering properties of elements and helium isotopes used in the modelling [1, 2, 8]. The values for the helium isotopes are taken from Fig. 1 at 1K. b is the bound coherent scattering length in femtometers (fm) [9]. SLD is the scattering length density defined as "Nb" where N is the number density of the material in question in atoms per Å^3 and b the bound coherent scattering length [7, 10].

This provides another contrast/dataset where all the elements bar the Helium are the same. We can then fit both sets of data simultaneously for each temperature. We can also obtain another contrast for just the Si block by changing the probe and using X-ray reflectometry from a lab-based source.

Supplementary Note 3: Modelling Methodology

The analysis was started using the simplest model possible. Once convergence was reached as defined in the *Refl1D* documentation [11], an assessment was made taking into account the improvement of the χ^2 and the uncertainty in the parameters as to whether to increase the complexity of the model by adding more parameters. We echo what is said in the *Refl1D* documentation [11] that, since this is a parametric modelling technique, we cannot say that any one model is truly correct, only that while it fits the observed data well, there may well be other possible solutions. We couple this knowledge with the following secondary information or criteria:

- A well-defined question or questions for what the modelling is intended to answer. This provides a measure of how well the model is working but, most

* oleg.kirichek@stfc.ac.uk

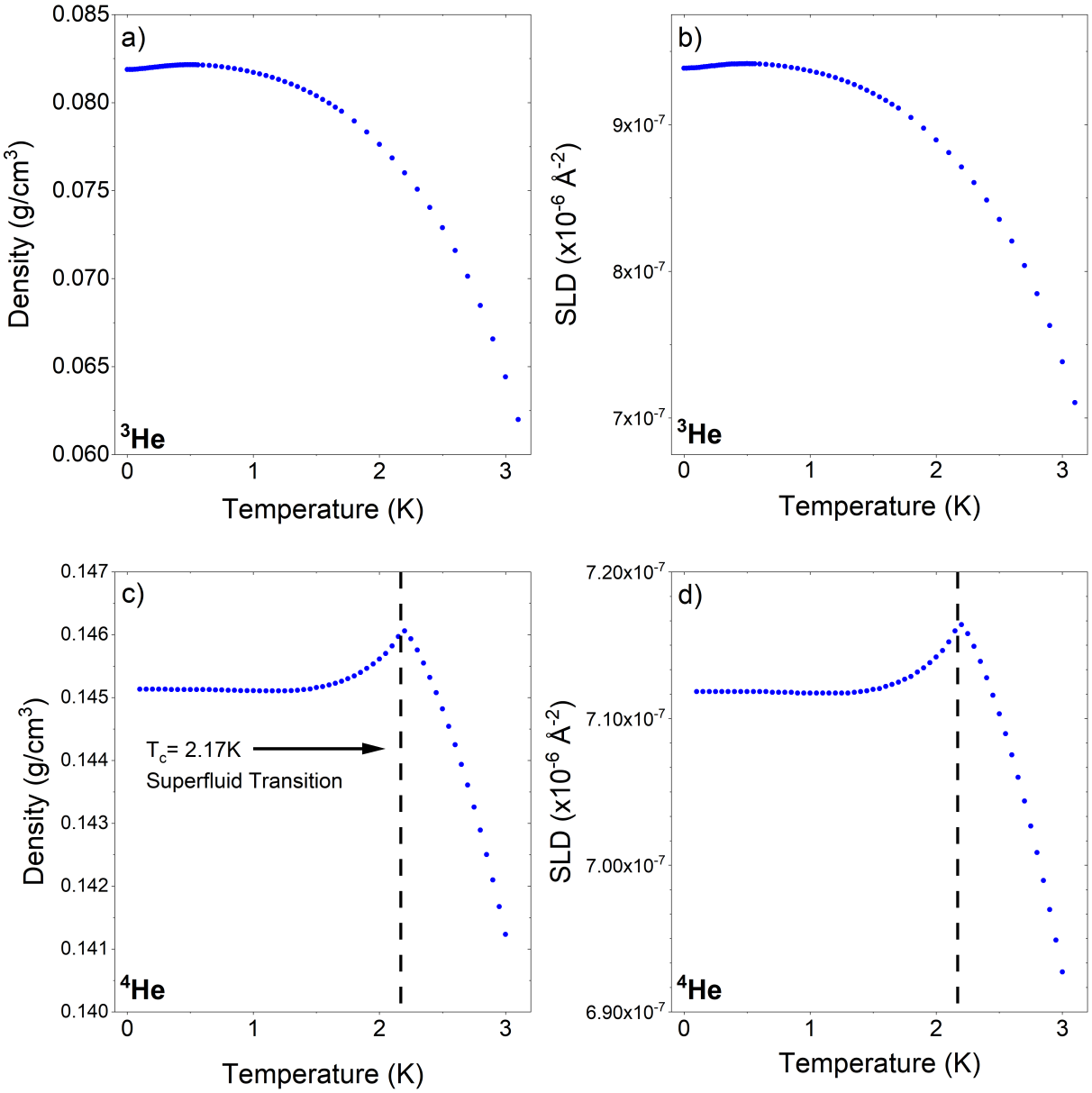

Supplementary Figure 1: Densities and scattering length densities as functions of temperature for ^{3}He and ^{4}He. Panel (a) shows density for ^{3}He as functions of temperature. Panel (b) shows density for ^{4}He as functions of temperature. Panel (c) shows scattering length density for ^{3}He as functions of temperature. Panel (d) shows scattering length density for ^{4}He as functions of temperature. These values were obtained from references [1, 2].

importantly, a point at which to stop fitting the data. It can also be instrumental in determining if the data quality is insufficient to answer the question posed.

- A knowledge of the sample growth conditions to provide initial priors (maximum and minimum bounds on those initial parameters) and a nominal starting structure. For example, the parameters of the substrate material should be well-known.

- Isotropic/magnetic/other contrast variation, which is akin to solving simultaneous equations. Standard isotropic contrast is not possible in this case. A second contrast for the Si block was obtained by measuring it with a vacuum in the cell, and a third via Cu K_α X-ray reflectivity on a separate lab-based source.

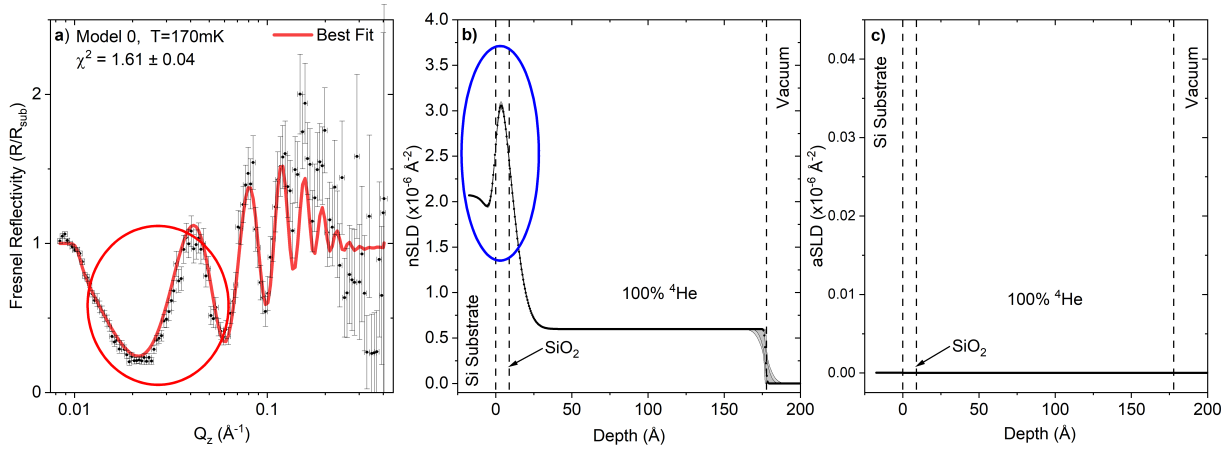

Supplementary Figure 2: Model 0: 170mK Single layer of pure ^{4}He. Panel a) shows Fresnel reflectivity. Panel b) shows Neutron Scattering Length density (nSLD) profile. Panel c) shows Neutron absorption profile (aSLD).

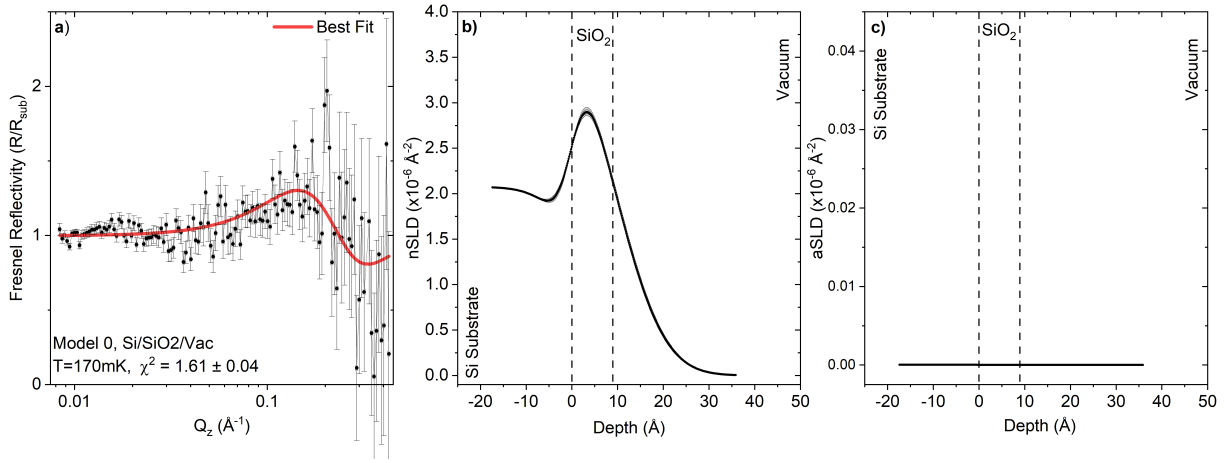

Supplementary Figure 3: Model 0: 170mK Si substrate/SiO2/Vacuum contrast. Panel a) shows Fresnel reflectivity. Panel b) shows Neutron Scattering Length density (nSLD) profile. Panel c) shows Neutron absorption profile (aSLD).

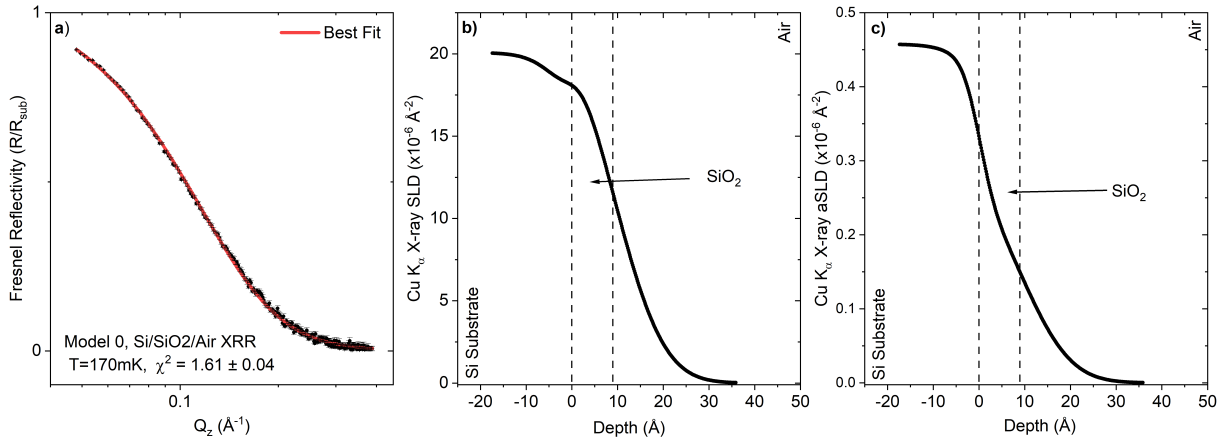

Supplementary Figure 4: Model 0: Room temperature X-Ray Si substrate/SiO2/Vacuum contrast. Panel a) shows Fresnel reflectivity. Panel b) shows X-Ray Scattering Length density (nSLD) profile. Panel c) shows X-Ray absorption profile (aSLD).

- Secondary characterization techniques, to provide a cross reference for a particular parameter and to lock them down, for example, atomic force microscopy for a minimum prior for the top surface roughness, or X-ray reflectivity for another contrast of the substrate/vacuum system.

Such information provides confidence in the validity of the model and avoids over-parameterization.

In this case, the questions are:

1. Can we measure a condensed liquid helium surface and layer on the Si block?
2. Can the model confirm the presence of dilute ^{3}He in the liquid ^{4}He both for nominally pure ^{4}He and for the 0.1%^{3}He-^{4}He mixture?
3. Can we determine the distribution of the ^{3}He as a function of temperature both for nominally pure ^{4}He and for the 0.1%^{3}He-^{4}He mixture?

To start the modelling process it is often best to start with the simplest model that describes the nominal system, *i.e.* the nominal structure that was specified in the sample growth. In this case, this is a silicon substrate with a thin SiO_2 layer and a layer of pure ^{4}He, referred to as model 0. The super phase above the helium is a vacuum.

To go beyond this simplicity and to constrain the modelling, the 170mK helium NR data were co-refined along with two other data sets. The first of these was an NR curve of the Si block on its own in the vacuum can, and the second was an X-ray reflectivity (XRR) curve of the Si block in Air. The XRR curve was obtained using a Rigaku SmartLab 9KW rotating anode x-ray diffractometer, using CuKα x-rays of wavelength 1.541Å. The XRR curve has had the critical edge data removed up to twice the critical angle to be able to model the data without systematic errors, due to the XRR footprint correction, dominating the fits. This often occurs when co-refining XRR and NR curves due to the much higher counting statistics of the XRR data, as modern lab sources are often orders of magnitude more intense than any neutron source. Time of flight neutron reflectometry does not have the same footprint systematic errors as it's possible to control the beam footprint and resolution at all angles to be the same, unlike a monochromatic measurement. The co-refinement shares as many parameters as possible. All subsequent fits of the temperature series data had these contrasts included to lock down the Si/SiO_2 parameters.

The aim of model 0 is to provide a null result as a baseline to justify any further increases in the complexity of the model. The results for model 0 are shown in Supplementary Figures 2, 3 and 4 for the Helium film and the Si block in a vacuum as measured by neutrons and x-rays respectively. Panel (a) of each figure displays the Fresnel reflectively (R_{Fresnel}) given by:

$$R_{\mathrm{Fresnel}} = \frac{R}{R_{\mathrm{Substrate}}}, \tag{1}$$

where the total reflectivity (R) is divided by the calculated substrate reflectivity ($R_{\mathrm{Substrate}}$). This aids visually in finding discrepancies between the fit and the data. In this case, the fit does not fully match the fringes' depth at low Q highlighted by the red circle in Supplementary Figure 2 (a).

Panel (b) shows the neutron/X-ray Scattering Length Density profile (nSLD). The greyed regions show the 68% and 95% Bayesian confidence intervals from the BUMPS fitting package. This gives some indication of how confident the model is with regard to the fit of the data, but we stress this just indicates how well the current model fits the data. It does not indicate whether the physical model is the correct one, or not. If the greyed regions matched the best-fit line perfectly then the model would have certainly to within 95% of reproducing the data.

Panel (c) shows the neutron/X-ray absorption scattering length density profile (aSLD). As the ^{3}He is the only isotope with appreciable neutron absorption in the whole system, this is a good indicator of where the ^{3}He is located as a function of depth.

The presence of Kiessig fringes[12, 13] in the data *unambiguously* shows the presence of a layer of helium, answering the first question of whether a layer of helium is present. Kiessig fringes arise due to constructive and destructive interference of the incoming and outgoing neutrons as they reflect from the film surface and the substrate/film (bottom-most) interface. This means they provide information on the total thickness of the film. Model 0 does a reasonable job of describing the system and reproducing the fringes, providing a layer thickness of 168 Å[166.83, 169.21]. The numbers in the brackets are the 95% Bayesian confidence intervals. However, there are many discrepancies, with the fit not following the data points well. The blue circle in Supplementary Figure 2(b), shows an anomaly where the roughness of the SiO_2 layer is greater than its width producing an over-described interface profile.

The next simplest model is to introduce 0.1%^{3}He to the ^{4}He layer to turn the layer into a mixture. Model 1, which is displayed in Supplementary Figure 5 consists of a single layer of helium on a Si substrate with a native SiO_2 layer between the Si bulk and the helium the same as model 0. The helium layer was modeled as a ratio of ^{3}He to ^{4}He in the form $^3\mathrm{He}_x^4\mathrm{He}_{1-x}$ where x was a fit-able parameter. The helium ratio was calculated and deliberately mixed to be a ratio of 0.1%^{3}He to ^{4}He when condensing the helium in the system. This improved the χ^2 as well as giving a measured ratio of ^{3}He to ^{4}He. The ratio (fitted between 0 to 1) worked out at 0.11 [0.070, 0.158] ^{3}He or 11% ^{3}He in the layer, a factor 10 bigger than the mixing ratio of 0.1% ^{3}He. Taking the Bayesian 95% interval into account this is statistically non-zero. This is displayed in the aSLD plot displayed in Supplemen-

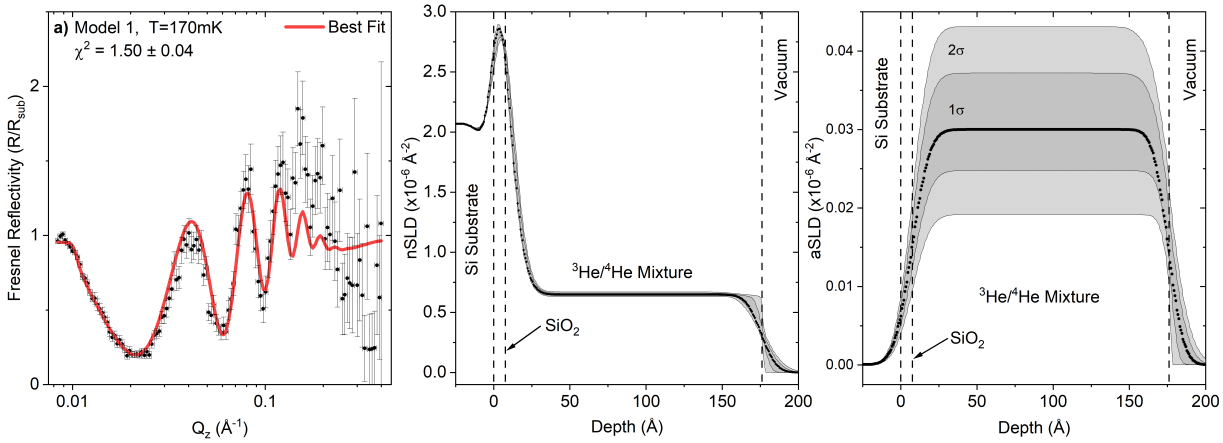

Supplementary Figure 5: Model 1: 170mK Single layer of ^{3}He^{4}He mixture/Vacuum. Panel a) shows Fresnel reflectivity. Panel b) shows Neutron Scattering Length density (nSLD) profile. Panel c) shows Neutron absorption profile (aSLD).

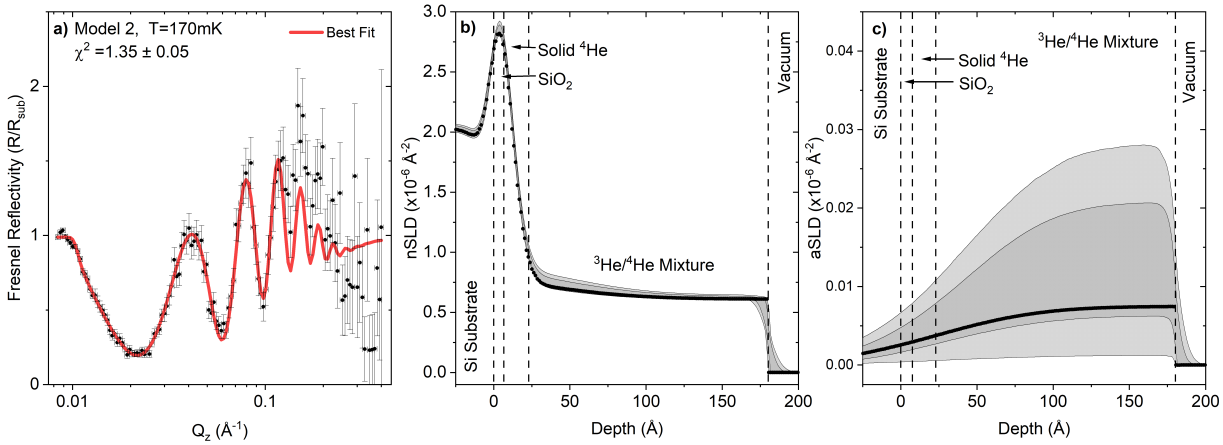

Supplementary Figure 6: Model 2: 170mK Solid thin layer of ^{4}He/ ^{3}He^{4}He mixture layer/Vacuum. Panel a) shows Fresnel reflectivity. Panel b) shows Neutron Scattering Length density (nSLD) profile. Panel c) shows Neutron absorption profile (aSLD).

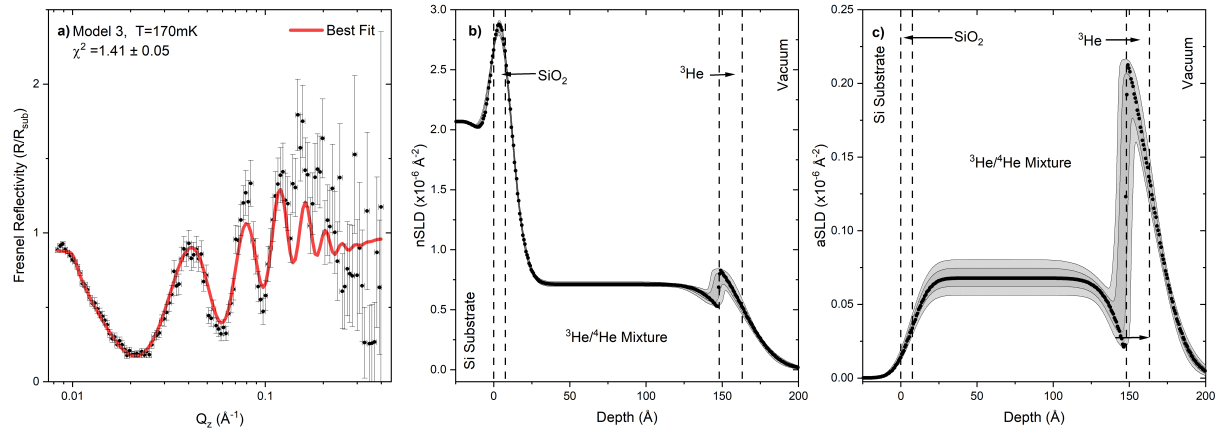

Supplementary Figure 7: Model 3: 170mK ^{3}He^{4}He mixture layer/thin ^{3}He layer/Vacuum. Panel a) shows Fresnel reflectivity. Panel b) shows Neutron Scattering Length density (nSLD) profile. Panel c) shows Neutron absorption profile (aSLD).

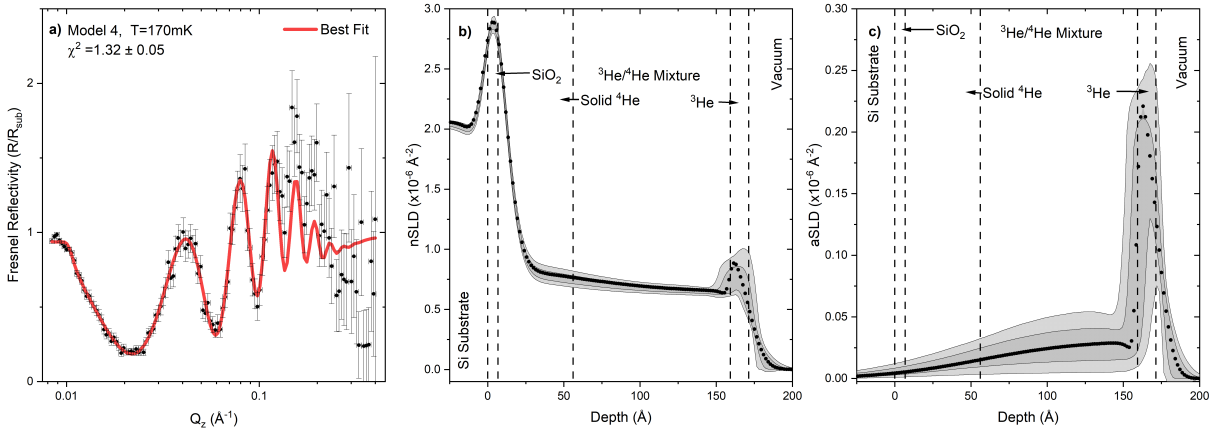

Supplementary Figure 8: Model 4: 170mK Solid thin layer of ^{4}He /^{3}He^{4}He mixture layer/thin ^{3}He layer/Vacuum. Panel a) shows Fresnel reflectivity. Panel b) shows Neutron Scattering Length density (nSLD) profile. Panel c) shows Neutron absorption profile (aSLD).

tary Figure 5(c). It's clear some absorption is required to improve the fit. This answers the first two questions posed above, of whether a helium layer can be resolved and whether ^{3}He can be detected within it.

Answering the third question regarding whether there is enough sensitivity in the data to detect a depth profile of ^{3}He through the helium film is more challenging. There are several pieces of information from the literature that we can use to guide us.

The first is from references [14, 15], where Lurio *et al* determined that there should be a solid ^{4}He layer at the interface between the substrate and the bulk of the helium film. This is incorporated into Model 2 as a pure ^{4}He layer with the initial density set to that of solid helium. This addition was found to dramatically improve the χ^2 as displayed in Supplementary Figure 6 (a). To get a reasonable fit to the data it was necessary to allow the roughness of the solid ^{4}He layer to exceed the size of the layer and expand into the bulk helium mixture layer, as shown in Supplementary Figure 6 (b); this allows the model to grade the density profile of the layer through the film showing a gradual decrease from the solid ^{4}He density to that of the mixture layer from model 1. This has the further effect of grading the aSLD profile such that there is more absorption towards the surface and less near the substrate, panel (c). This agrees with the theory of ^{3}He layer phase separation towards the surface as well as a solid ^{4}He layer at the interface with the substrate as observed by Lurio *et al*. However the ratio of ^{3}He/^{4}He in the bulk is reduced to a low value ≈ 0.03 [0.00, 0.11] ($\approx 3\%$), which is not in agreement with the amount of ^{3}He added to the system. But with a non-uniform ^{3}He distribution it would not be expected that the absolute value would match that of a uniform distribution with low regions being balanced out by higher ones; however, the profile in panel (c) is significantly lower across the board.

We therefore put model 2 to the side and take account of the second piece of information, that theory predicts an increase of ^{3}He towards the surface at temperatures $T < 1$ K [16–18]. Model 2 hints that the fit would be better if this was the case.

Model 3 puts this to the test by adding a ^{3}He layer at the surface with no solid ^{4}He layer at the substrate interface. This helium layer is a fixed density ^{3}He layer, set for bulk ^{3}He see Supplementary Table I.The thickness and roughness of this layer are allowed to vary from zero Å to a large number. The results are displayed in Supplementary Figure 7. The χ^2 improves slightly but produces a non-physical nSLD profile at the interface between the mixture layer and the ^{3}He layer and a similar anomaly in the aSLD profile. The isotopic ratio was allowed to vary between being fully ^{3}He and fully ^{4}He. Model 3 produces a non-physical fit near the surface but does show an improvement of the fit by introducing a ^{3}He rich layer at the surface in line with the predictions of Krotscheck *et al* [16]. We note that the fit does not try to remove the ^{3}He layer by setting the thickness to zero, so this is again hinting at a density increase towards the surface.

The next step is to combine models 2 and 3 by introducing both a thin solid ^{4}He layer at the substrate interface as well as a thin ^{3}He rich layer at the surface. This yields Model 4 as displayed in Supplementary Figure 8. It produces the lowest χ^2 of all the fits so far, and reasonable nSLD and aSLD profiles, removing all anomalies bar the over-described roughness of the Si substrate/SiO_2 interface. The thin ^{4}He layer is graded out to produce a slightly downward-sloped density profile into the bulk of the mixture layer, that slopes down in nSLD until close to the surface where there is a small peak in nSLD due to the ^{3}He rich layer of thickness $\sim$15Å [13, 19]. This would be indicative of a density change, not a sharp thin

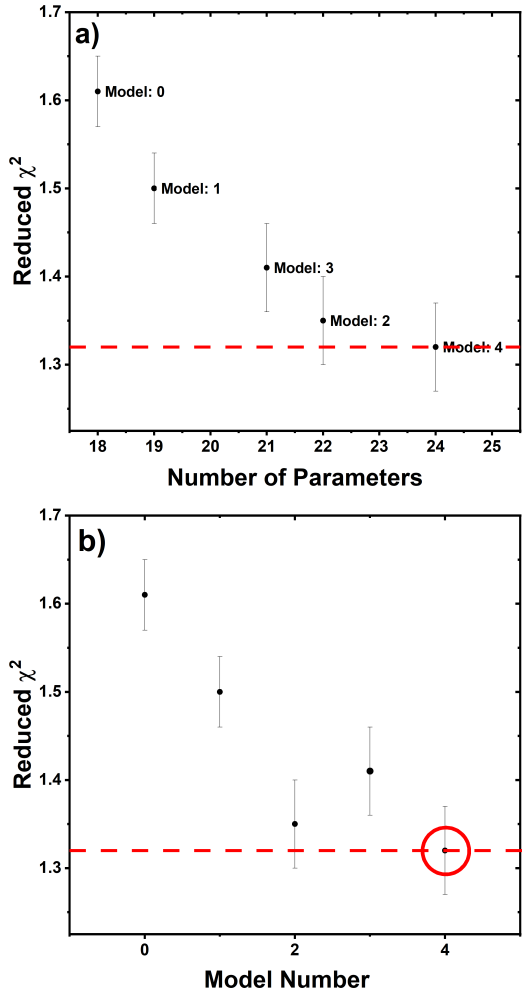

Supplementary Figure 9: Comparison among various models. Panels a) and b) have the trends of reduced χ^2 vs the number of parameters and model number respectively. The dashed red line is a guide to the eye showing the level of model 4 which has the lowest (best) χ^2 value.

solid ^{4}He layer as in refs [14, 15]. We also note that none of the interfaces is near atomic sharpness as predicted in the work of Krotscheck *et al*, and we speculate that this may be due to the vibrations of the E-18 fridge pulse tube. We cannot definitively state that the region is indeed solid ^{4}He but can state the model needs to put something slightly denser up against the SiO_2 layer as compared to the bulk ^{3}He/^{4}He mixture layer. We note that while the mixture layer is graded it has a similar density value to that of model 2, which is in good agreement with the experimental mixing.

The various models are summarized in Supplementary Figure 9. It's clear that model 2, with a simple mixture layer, does a good job of reproducing the data. However, we are confident that the increase in complexity of model 4, with its slight improvement of χ^2, allows the ^{3}He distribution to be approximately depth-profiled, thereby answering the third-stated question above. At this point, model 4 was used to analyse the other temperature data sets, the nSLD and aSLD plots from this fitting are displayed in the main text and the reflectivity fits and SLD plots are also displayed in Supplementary Figure 10. It should be noted model 4 did not work at all for the 300 mK data set. At this temperature, the model had to be changed from three layers to one very thin ^{3}He layer at the SiO_2 interface. The priors were allowed to go to an extreme thickness. This allowed for the fact that a similar smoothing of the curve could result from a layer that goes thicker than the beamline resolution can resolve. However, the model always produced a very thin layer. This simpler model reproduced the data, however it still produced a non-physical nSLD profile. We did not manage to find an ideal box model solution that physically fit the 300 mK data set. This coupled with the off-specular work mentioned in the main text leads us to believe that there is only a partial layer at best on the surface of the silicon block at 300 mK.

The commercial helium data did not require the same level of complexity as the 0.1%^{3}He/^{4}He mixture data. In this case, the model did not need the ^{3}He rich surface layer. Model 2 was sufficient to analyse the data. The helium mixture ratio was ultimately set to be pure ^{4}He as the fit did not vary the ratio meaningfully below 100% ^{4}He. This simplified the model further. This analysis is displayed in Supplementary Figure 11. It should be noted there is very little change between all the ^{4}He curves, but there is a lot of uncertainty on the plots as shown by the Bayesian 95% confidence intervals that are quite broad at the surface and substrate/SiO_2 interfaces. These confidence bounds are all overlapping showing to the 2σ (95%) limit that the nSLD curves are all indistinguishable. There are two primary reasons we can think of for the large uncertainties on the nSLDs as compared to the 0.1%^{3}He/^{4}He nSLDs. The first is that the commercial helium data has far fewer features in it as compared to the mixture data, so there is a lot less information for the fits to lock in on. The second is that the commercial helium data was taken one year before the mixture data when the passive vibration damping was not as good on the E18 cryostat system. This could also be causing the smearing out of the interfaces from the fits.

Suffice it to say the main conclusion from the commercial ^{4}He case is that no ^{3}He was required to fit the data in the mixture layer or at the surface, hence the use of a simplified Model 2. More importantly, there appears to be little or no change as a function of increasing temperature with perhaps a slight increase in the diffuse nature of the surface interface with increasing temperature.

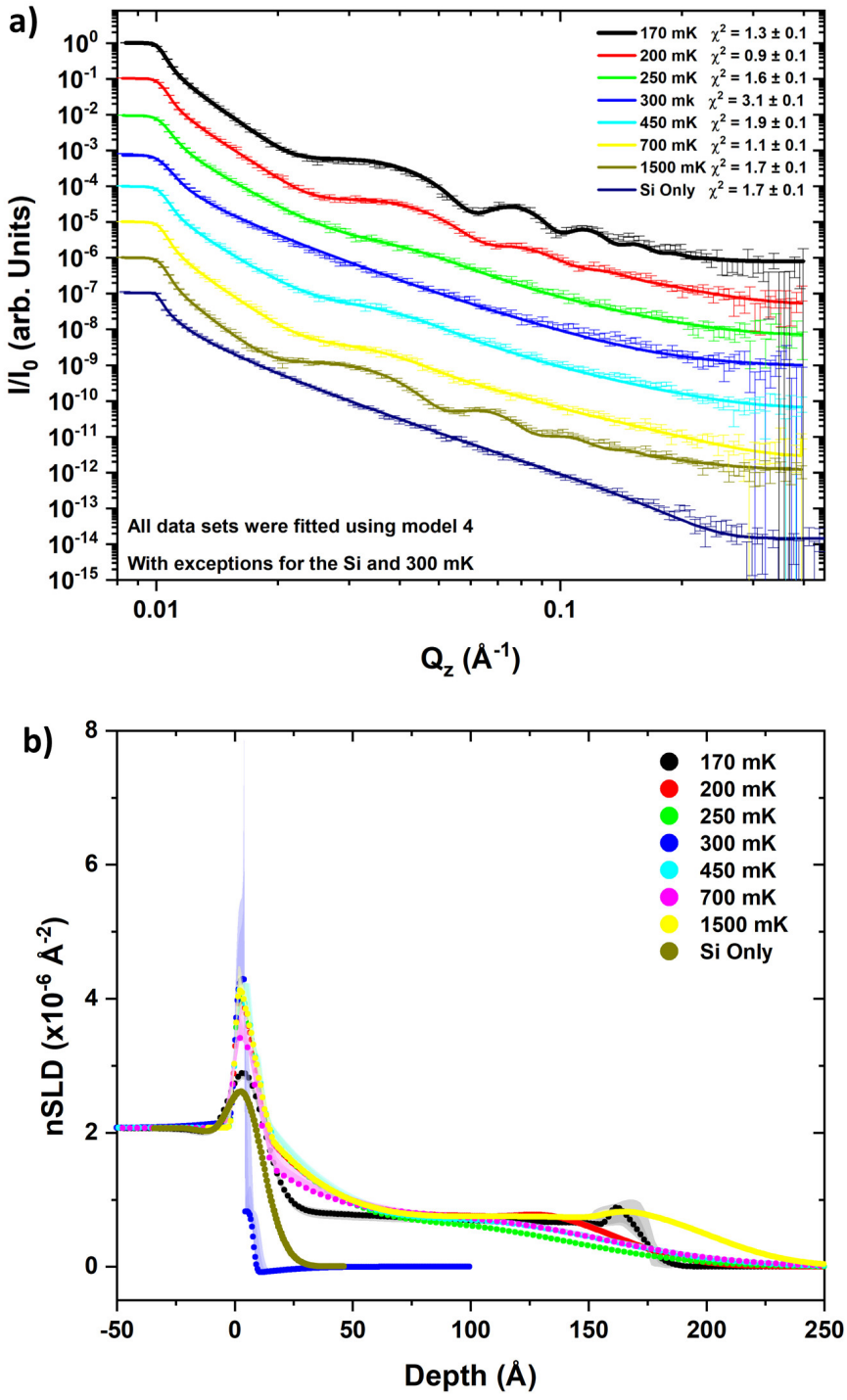

Supplementary Figure 10: Reflectivity fits and nSLD plots for the mixture film. Panel (a) displays the Reflectivity data along with the best-fit curves for the various temperatures all offset from each other, it's clear to see the change in the curves from the presence of a layer of helium as evidenced by the Kiessig fringes, to their disappearance and the loss of the helium layer at 300mK and their reappearance of the layer and Kiessig fringes as the temperature approaches 1500 mK. Panel (b) the nSLD plots overlaid on top of each other to show the changes. The shaded region shows the Bayesian 95% confidence intervals while the solid lines show the best fits.

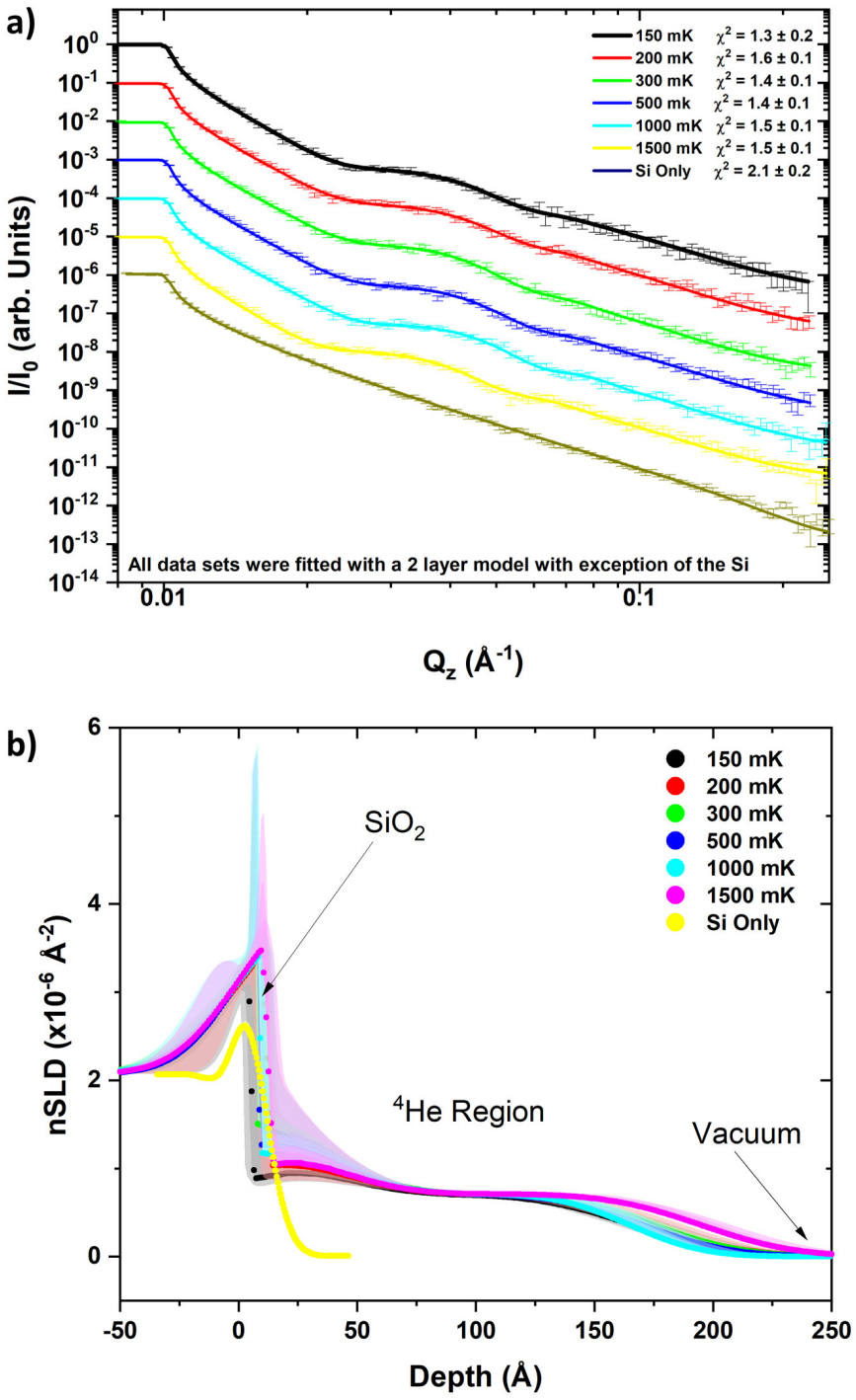

Supplementary Figure 11: Reflectivity fits and nSLD plots for the commercial Helium. Panel (a) displays the Reflectivity data along with the best-fit curves for the various temperatures all offset from each other for the commercial Helium, this was done using a simplified version of model 2. Panel (b) the nSLD plots overlaid on top of each other to show the changes. In this case, there is very little change with all variation being within the confidence intervals and therefore indistinguishable to the 2σ level. The shaded regions show the Bayesian 95% confidence intervals while the solid lines show the best fits.

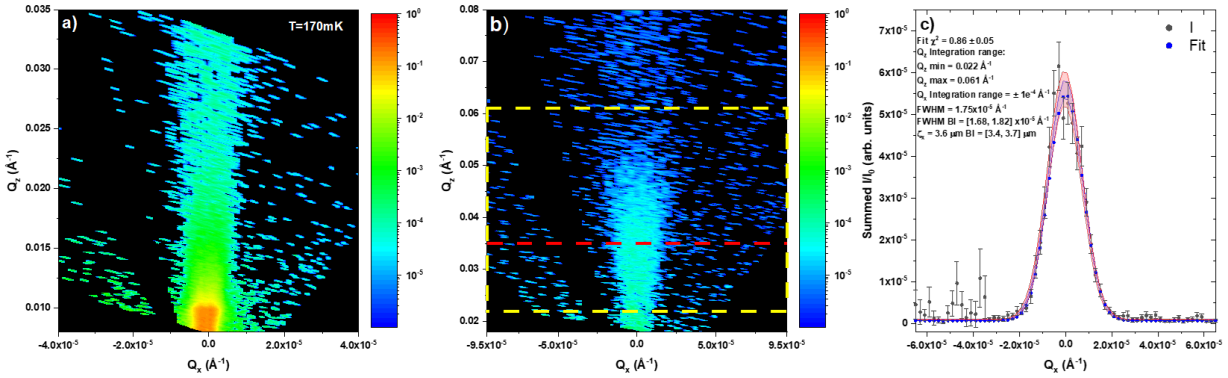

Supplementary Figure 12: Off-specular maps of 0.1% ^{3}He/^{4}He mixture at 170mK. Panel a) shows $Q_X Q_Z$ map at the lowest time of flight measurement angle capturing the critical edge. Panel b) shows second time of flight angle showing the overlap with the first angle as indicated by the red dashed line. The yellow dashed square shows the integration range around the first Kiessig fringe. Panel c) shows Pseudo rocking curve from the integration with Bayesian Gaussian fit.

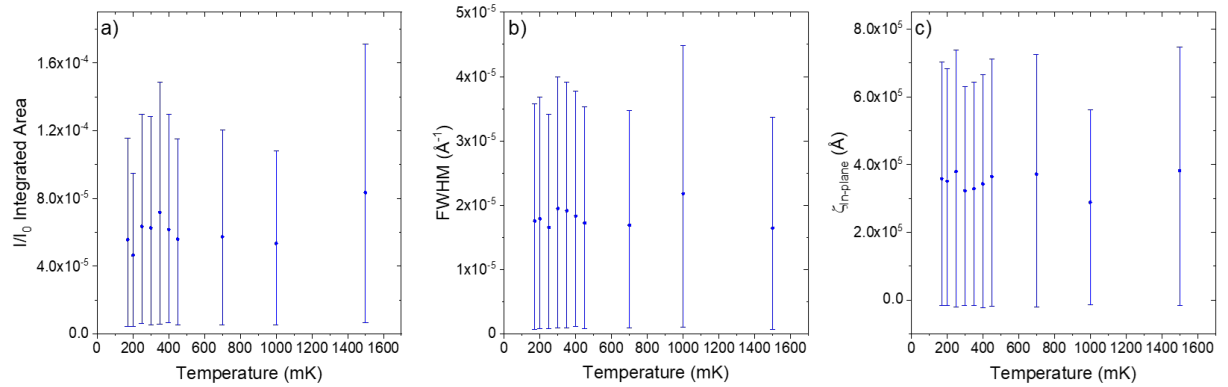

Supplementary Figure 13: Results of the fitting of the pseudo-rocking curve analysis as a function of temperature. Panel a) shows the integrated intensity, shows no variation within the error bar. Panel b) shows the FWHM also shows no variation within the error bar. Panel c) shows the conversion from FWHM to lateral in-plane correlation length showing a fairly stable in-plane correlation length of $\approx 4\mu$m well below the in-plane coherence length of the POLREF beamline of $\approx 50\mu$m

.

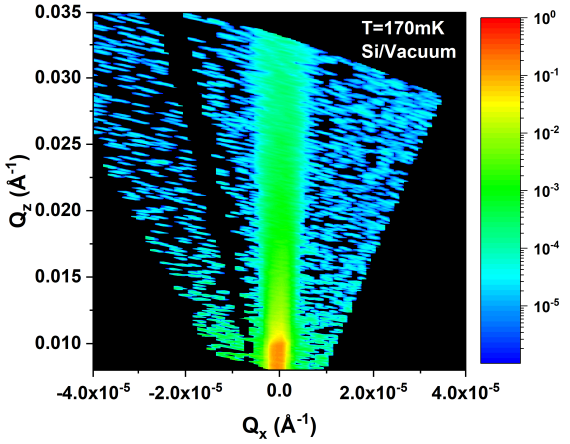

Supplementary Figure 14: The scattering from the Si block with no helium present, in vacuum at 170mK. A clear, sharp specular reflection is seen.

Supplementary Note 4: Future directions for Specular Reflectivity work

Several avenues can be taken to both improve the measurements and analysis of this type of system as well as science directions that we strongly feel are worth exploring:

Starting with the experimental setup, a lot of work was done between the commercial helium and 0.1%^{3}He mixture experiments to passively damp vibrations due to the pulse tube cryocooler and from the surrounding beamline. We strongly suspect that while we saw an improvement due to our efforts there is a lot more to be done. We suspect much better results can be obtained by implementing an active damping scheme akin to the work of den Haan *et al* [19], where active damping was used to perform atomic resolution scanning tunnelling microscopy in a cryogen-free dilution refrigerator. This may significantly improve the data quality via film stability.

The methodology of the measurement can be improved in ways that can aid the analysis by the addition of a thick reference layer such as deliberately making a 200nm thick SiO_2 layer rather than a native SiO_2 layer. This layer could be anything as long as it is high contrast as compared to the Si substrate and the helium. This works to boost the signal in a way analogous to a radio carrier signal, by introducing a high-frequency modulation at low Q_z, where the statistics are highest. This high frequency is then very sensitive to any envelope function that is provided by any thinner layers such as thin ^{3}He surface-rich regions or suspected solid ^{4}He layers at the substrate interfaces. It has been used before in the literature most recently to study monolayer graphene by Aboljadayel *et al* [20].

The contrast could be further boosted by adding a magnetic reference layer coupled with a thick overlayer and polarised neutron reflectivity (PNR). This magnetic contrast method has been extensively used in the soft matter community [21, 22] and reduces the ambiguity of the fitting. The use of the above three methods could be a way forward to further improve the present work.

However, we do hope this work shows the utility of Neutron reflectivity to the study of Helium and its isotopes.

Supplementary Note 5: Off-Specular Data Analysis

To provide a better understanding of what was occurring during the disappearance of the helium film at 300mK the off-specular maps were examined. The POLREF beamline has a linear detector with an angular range of 3 degrees, that is normally summed to produce a specular data set. However, this data can be converted to a Q_x-Q_z map, examples of which are shown for the first two incident angles of the 170mK 0.1% ^{3}He data set in Supplementary Figure 12. As shown in the main text it is clear that there is an increase in the off-specular scattering around the specular ridge. To quantify this, the pseudo rocking curves were created by integrating in Q_z around the first Kiessig fringe as shown by the yellow dashed box in Supplementary Figure 12 (b). The result of this is shown in Supplementary Figure 12(c). The BUMPS package [4] was then used to fit a Gaussian to this rocking curve to obtain the integrated intensity and the Full Width Half Maximum (FWHM). The correlation length η corresponds to an in-plane length scale on the surface where the correlation function between the two points is reduced to a value of 1/e [23], giving an estimate of the probability of finding another point of height z within a distance x at any position on the sample surface.

The result of this simple analysis is shown in Supplementary Figure 13 and clearly shows that for all temperatures the specular ridge is very similar: there is no variation in temperature within the error bar. This strongly implies that the broadening down by the critical edge comes about through sources other than off-specular reflectivity from the helium film or the silicon block.

Finally, we present the scattering from the Si substrate at 170mK with no helium present (Supplementary Figure 14). The scattering is intense and sharp in Q_x. These data are consistent with the measurements for helium present at 300mK, *i.e.* there is no evidence of off-specular scattering. The high intensity of the critical reflection is consistent with the absence of the thin absorbing ^{3}He film we see at 300mK when some ^{3}He is present on the surface.

SUPPLEMENTARY REFERENCES

[1] E. C. Kerr and B. J. Taylor, Molar volume and expansion coefficient of liquid ^{3}He, Ann. Phys. **20**, 450 (1962).

[2] E. C. Kerr and R. D. Taylor, The molar volume and expansion coefficient of liquid ^{4}He, Ann. Phys. **26**, 292 (1964).

[3] P. Kienzle, B. Maranville, K. O'Donovan, J. Ankner, N. Berk, and C. Majkrzak, `https://www.nist.gov/ncnr/reflectometry-software` (2017).

[4] P. Kienzle, J. Krycka, N. Patel, and I. Sahin, `https://bumps.readthedocs.io/en/latest/` (2011).

[5] F. Abelés, La théorie générale des couches minces, J. Phys. Radium **11**, 307 (1950).

[6] L. Névot and P. Croce, Caractérisation des surfaces par réflexion rasante de rayons x. application a l'etude du polissage de quelques verres silicates., Rev. Phys. Appl. **15**, 761 (1980).

[7] D. S. Sivia, *Elementary Scattering Theory for X-ray and Neutron Users* (Oxford University Press, 2011) chapter 4:.

[8] P. A. Sheldon and R. B. Hallock, Properties of 2D ^{3}He on very thin ^{4}He films, Phys. Rev. Lett. **77**, 2973 (1996).

[9] D. J. Bishop and J. D. Reppy, Study of the superfluid transition in two-dimensional ^{4}He films, Phys. Rev. B **22**, 5171 (1980).

[10] National centre for neutron research scattering length database, `https://www.ncnr.nist.gov/resources/n-lengths/` (2021).

[11] P. Kienzle, J. Krycka, N. Patel, and I. Sahin, `https://refl1d.readthedocs.io/en/latest/guide/fitting.html#reporting-results` (2017).

[12] H. Kiessig, Interferenz von röntgenstrahlen an dünnen schichten, Annalen der Physik **402**, 769 (1931).

[13] J. Als-Nielson and D. McMorrow, *Elements of Modern X-Ray Physics* (Wiley, 2001).

[14] L. B. Lurio, T. A. Rabedeau, P. S. Pershan, I. F. Silvera, M. Deutsch, S. D. Kosowsky, and B. M. Ocko, Liquid-vapor density profile of helium: An X-ray study, Phys. Rev. Lett. **68**, 2628 (1992).

[15] L. B. Lurio, T. A. Rabedeau, P. S. Pershan, I. F. Silvera, M. Deutsch, S. D. Kosowsky, and B. M. Ocko, Liquid-vapor density profile of helium: An X-ray study, Phys. Rev. Lett. **72**, 309 (1994).

[16] E. Krotscheck, M. Saarela, and J. L. Epstein, Impurity states in liquid-helium films, Phys. Rev. B **38**, 111 (1988).

[17] D. O. Edwards, S. Y. Shen, J. R. Eckardt, P. P. Fatouros, and F. M. Gasparini, Propagation of surface sound in superfluid ^{3}He-^{4}He, Phys. Rev. B **12**, 892 (1975).

[18] R. M. Heinrichs and R. B. Hallock, Temperature-dependent third sound velocity measurements in ^{3}He-^{4}He films, in *Helium-75*, edited by J. G. M. Armitage (World Scientific, Singapore, 1983) pp. 40–41.

[19] A. M. J. den Haan, G. H. C. J. Wijts, F. Galli, O. Usenko, G. J. C. van Baarle, D. J. van der Zalm, and T. H. Oosterkamp, Atomic resolution scanning tunneling microscopy in a cryogen free dilution refrigerator at 15 mK, Review of Scientific Instruments **85**, 035112 (2014).

[20] R. O. M. Aboljadayel, C. J. Kinane, C. A. F. Vaz, D. M. Love, R. S. Weatherup, P. Braeuninger-Weimer, M.-B. Martin, A. Ionescu, A. J. Caruana, T. R. Charlton, J. Llandro, P. M. S. Monteiro, C. H. W. Barnes, S. Hofmann, and S. Langridge, Determining the proximity effect-induced magnetic moment in graphene by polarized neutron reflectivity and x-ray magnetic circular dichroism, ACS Applied Materials & Interfaces **15**, 22367 (2023).

[21] A. Koutsioubas, Model-independent recovery of interfacial structure from multi-contrast neutron reflectivity data, Journal of Applied Crystallography **52**, 538 (2019).

[22] C. F. Majkrzak, N. F. Berk, and U. A. Perez-Salas, Phase-sensitive neutron reflectometry, Langmuir **19**, 7796 (2003).

[23] T. P. A. Hase, J. D. R. Buchanan, B. K. Tanner, S. Langridge, R. M. Dalgliesh, S. Foster, C. H. Marrows, and B. J. Hickey, Resonant magnetic X-ray and neutron diffuse studies of transition metal multilayers, J. Appl. Phys. **93**, 6510 (2003).